

Post Access Report

Optimization of Fairing Geometry for ORPC Modular RivGen
Power System

Awardee: Ocean Renewable Power Company

Awardee point of contact: Matthew Barrington

Facility: National Renewable Energy Laboratory

Facility point of contact: Will Wiley

Date: 8/12/2024

1 INTRODUCTION TO THE PROJECT

ORPC designed and built a modular fairing for the Modular RivGen® MHK turbine, which accommodates the efficient deployment and operation of turbine arrays. The modular support also acts to augment the flow into the rotor for increased power production. This work aims to optimize the hydrodynamic performance of the flow augmentation using a computational fluid dynamics (CFD) study. The influence of two geometric parameters was assessed: the fairing cross-sectional shape and the rotor-fairing spacing. In addition to net power, the analysis looked at discretized loading of the turbine components, to evaluate both ultimate and fatigue loads.

The numerical modeling used the commercial CFD code, Star-CCM+ and the open-source code OpenFOAM. This code-to-code verification was intended to increase confidence in the results and in the use of open-source tools for high fidelity marine energy modeling. The use of OpenFOAM also took advantage of an actuator line library, turbinesFoam.

2 ROLES AND RESPONSIBILITIES OF PROJECT PARTICIPANTS

The applicant (ORPC) and the facility (NREL) worked together to find a fairing geometry that balances optimal hydrodynamic performance and practical construction.

2.1 APPLICANT RESPONSIBILITIES AND TASKS PERFORMED

ORPC provided the rotor design, inflow conditions, and operating conditions to be used in the analysis, based on the Modular RivGen Power System. This includes the depth, width, and shape of the domain and the inflow velocity and profile. They also provided the base modular fairing geometry as the starting point for the optimization.

ORPC defined practical limits for the parameter ranges. This includes the maximum height of the fairing, from top to bottom, constraining the spacing between the rotor and the fairing. This also includes limitations on cross-section shape for constructability. This could include limitations on the amount of curved surfaces and minimum thicknesses.

ORPC also provided guidance and limits based on the ability to combine units into an array.

2.2 NETWORK FACILITY RESPONSIBILITIES AND TASKS PERFORMED

NREL performed the CFD analysis. NREL and ORPC determined the matrix of geometries to evaluate. NREL justified the numerical schemes and levels of spatial and temporal discretization used in the work. NREL used the high-performance computing systems, Eagle and Kestrel, to perform the computations.

NREL post-processed the simulations to evaluate each geometric iteration based on net power, ultimate loading on the blades and struts, and fatigue loading on the blades and struts.

3 PROJECT OBJECTIVES

The primary aim of this work was to improve the hydrodynamic performance of the modular RivGen MHK turbine. Cross-flow turbines experience complex dynamic flow heavily influenced by boundary layer effects, wake interactions, dynamic stall, high angles of attack, and vortex shedding. The optimal flow augmentation from a duct is less straight-forward than an axial flow turbine, and reduced order modeling is not capable of accurately predicting the hydrodynamic performance and detailed load progression. Not only is the net increase in mass flow through the rotor region important, but also the impact on the pressure distribution on the foils near the duct and the influence on dynamic stall. The findings from this high-fidelity numerical work are meant to inform the specific design for the RivGen turbine, and also provide qualitative knowledge for general cross-flow turbine ducts. Designs were evaluated based on net power production in addition to ultimate and fatigue load on individual blade sections. The outcome of this study aims to develop an improved low-cost system for tidal and riverine applications. The knowledge gained is meant to inform future ORPC fairing designs for increased power production.

Each geometry iteration was evaluated on three criteria: the power coefficient, the maximum load on the blades at the strut connections, and the fatigue load on the blades at the strut connections.

An optional second goal was to perform a code-to-code verification to help validate the use of open-source codes in MHK modeling. The use of open-source tools provides more accessibility to the marine energy community to perform high-fidelity analyses.

4 TEST FACILITY, EQUIPMENT, SOFTWARE, AND TECHNICAL EXPERTISE

The commercial CFD software STAR-CCM+ was run on NREL's high-performance computing systems, Eagle and Kestrel. This configuration has been used for previous CFD work for ORPC, and the project can take advantage of knowledge and practices from the prior projects.

The NREL marine energy team has experience with this turbine and was able to leverage previous results to inform the modeling in this work. Spatial and temporal discretization convergence studies were previously performed for the turbine. The resulting numerical setup for the rotor was used again here. The numerical setup for the base support was also be used as a starting point for the support modeling. NREL also has experience analyzing the performance of this turbine and used previously generated methods of quantifying the hydrodynamic loads. This experience allowed a more efficient project and an increase in confidence in the results.

5 TEST OR ANALYSIS ARTICLE DESCRIPTION

The ORPC RivGen Power System is an industry leading riverine cross-flow turbine. The turbine was deployed in Igiugig, Alaska and was the “longest operating marine energy project in all of the Americas” (ORPC, 2023). This turbine had a rated power of 40 kW at a current speed of 2.25 m/s and 80 kW at a current speed of 3.5 m/s (ORPC, 2023). The turbine is designed to provide clean renewable energy to communities without disturbing their waterways or the ecosystems in them.

The turbine features three helical blades and three struts for each of two rotors. The RivGen Power System is shown in the figure below.



Figure 1. RivGen Power System (ORPC, 2023)

ORPC designed a modular support for the turbine which allows for an efficient deployment of turbine arrays. The support also acts to augment the flow into the turbine for improved power production.

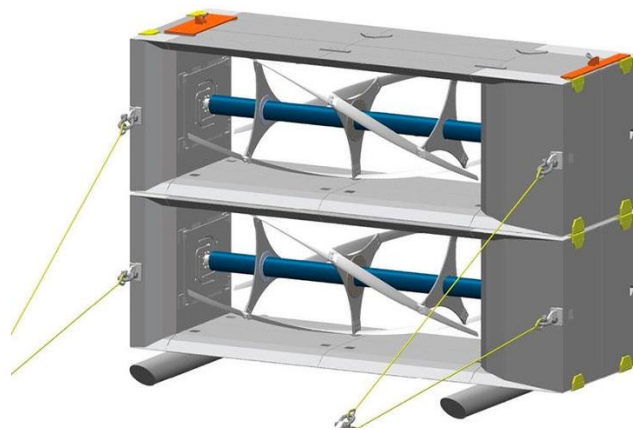


Figure 2. Modular RivGen Power System (Garanovic, 2022)

The base modular support fairing was used in a prior CFD study. Possible improvements to the flow augmentation were identified, and this work will iterate from the base geometry to improve the flow changes due to the fairing.

6 WORK PLAN

6.1 NUMERICAL MODEL DESCRIPTION

The numerical methods used were based on previous CFD modeling of the ORPC RivGen Power System by NREL. Both spatial and temporal convergence studies were already performed for the base system, and the resulting setup was used here. Sufficient and efficient refinement levels for the rotor, support, wake, and free surface had been found and did not change.

Star-CCM+ was the main tool used for numerical modeling. This commercial code is licensed and maintained by Siemens, and it is widely used and verified in the marine energy and general hydrodynamics communities. NREL performed a Reynolds averaged Navier Stokes analysis with an unsteady second order implicit time scheme, and with second order upwind convection for velocity and turbulence. Cross-flow turbines have inherently unsteady flow, so this time approach is critical. The presence of helical blades, the importance of strut interactions, and the three-dimensional (3D) flow augmentation of the support, all make a full 3D model important. A larger initial geometry sweep was done with a two-dimensional (2D) domain, and a select number of cases were run with a 3D domain.

Dynamic stall occurs twice for each foil during each turbine revolution due to the rapidly changing angle of attack. This phenomenon significantly changes the loading of the blades. The ability for the boundary layer to stay attached to the foil is strongly influenced by turbulence, and so it is important for turbulence to be modeled in some way. Turbulence in the free shear is also important when the blades on the downstream stroke pass through the wake of the upstream stroke. The previous CFD work on this turbine performed by NREL assessed multiple options, and selected a $K-\omega$ SST model; this was used again. In addition to the turbulence, the boundary layer mesh is also critical for the prediction of dynamic stall. Y^+ values on the foils was kept within the viscous sublayer for all blade-resolved simulations.

The motion of the rotor was modeled with a rotating fluid region within a stationary fluid region, connected by a cylindrical sliding interface for all blade-resolved simulations. The rotating region used a polyhedral mesh to accommodate the complex geometry of the rotor and continually changing orientation of cells with respect to the mean flow. The outer stationary region used a hexahedral mesh aligned with the mean flow, allowing efficient refinement of the free surface region. The volume of fluid method will be used to model the free surface with incompressible constant density water and air phases. It has been previously found that capturing the correct hydrostatic pressures can have important effects on the foil loads.

6.2 TEST AND ANALYSIS MATRIX AND SCHEDULE

Previous CFD work found that the flow augmentation of the modular support was not ideal for net power production. This optimization study will adjust the top and bottom cross-section shapes using both simple geometric fairings and NACA foil sections. The set of sectional shapes to test will be decided as the first step of this work. Limitations on the cross-section shape will be set by ORPC based on construction and transportation limitations. Preliminary limitations are a total vertical height of 2.5 m and a total horizontal length of 2.4 m. Depending on the trends identified ORPC is interested to know the possible performance gains from exceeding these limitations.

A preliminary set of geometries is shown in the table below based on 4-digit NACA foil sections. The first set of simulations will be done in 2D where computational efficiency will allow the modeling of many iterations. These results will identify the regions of the design space with the most potential and identify which design variables the loads are most sensitive to.

2D 4-Digit NACA Foil Sections

	minimum	maximum	points	
chord length	2.00	2.40	4	[m]
maximum camber	0.00	5.00	4	[% chord]
position of maximum camber	40.00	60.00	3	[% chord]
thickness	8.00	15.00	4	[% chord]
angle of attack	0.00	8.00	4	[deg]
horizontal position	-1.40	-1.00	4	[m downstream of shaft]
vertical spacing	2.00	2.30	4	[m]

1006 of 12288 fit inside geometric constraints

Table 1. Preliminary 2D 4-digit NACA foil section test matrix

The table above results in 12288 options; of those options only 1006 fit within the geometric constraints. In addition to total height and width, the geometries cannot interfere with the rotor area. The figure below shows a subset of the allowable foil shapes and the geometric constraints. The horizontal position from the table is labeled with “XF”, and the vertical spacing from the table is labeled with “SF”.

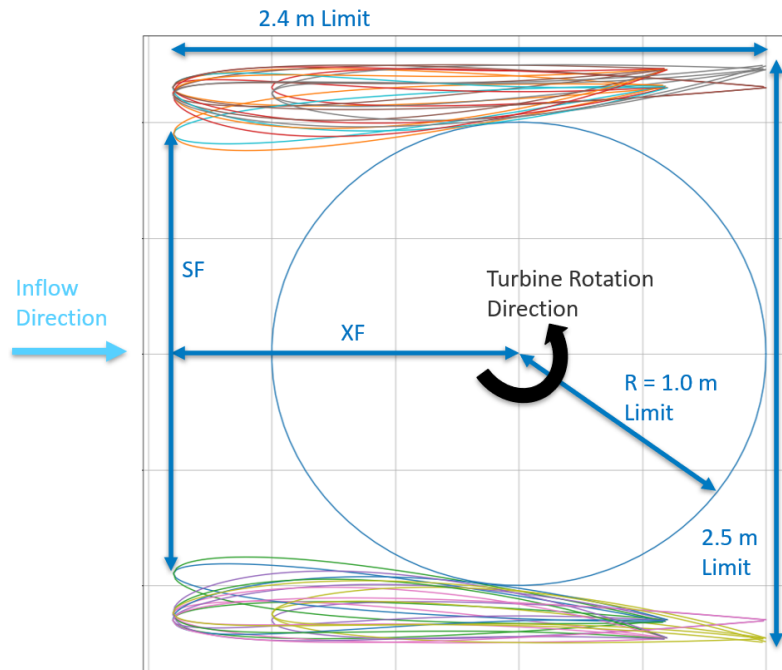


Figure 3. Support dimension variables and constraints showing subset of allowable configurations

In the original modular fairing design, the clearance to the passing foil is very small contributing to large interference effects on the foil pressure distribution. This gap will be given special consideration. For all design iterations the flow field will be qualitatively assessed to make sure that refinement regions around the support capture the specific dominating effects of the unique fairing.

The effects of the design parameters are not independent. As specific flow patterns are identified, the subsequent fairing designs will be adjusted accordingly. A gradient based optimization scheme will also be considered, with an output goal set of power coefficient, maximum ultimate load, and maximum fatigue load.

Depending on the identified trends, geometries beyond NACA foil sections will also be considered. Control points will be used to adjust the cross-section shape using spline tools.

Results from the set of 2D simulations will identify key geometries to simulate in 3D. The most promising configurations will be run in 3D, and variations of the parameters leading to the highest sensitivity will be tested.

ORPC wants to learn about the highest potential performance of their system. If unexpected trends are identified in this project, the possible set of geometries should not be constrained to this preliminary test matrix.

The following Gantt Chart has been updated to show the in-testing adjustment of the parameter ranges, following the analysis of the initial iterations.

	March				April				May				June				July				August				September			
Tasks	WK1	WK2	WK3	WK4	WK5	WK6	WK7	WK8	WK9	WK10	WK11	WK12	WK13	WK14	WK15	WK16	WK17	WK18	WK19	WK20	WK21	WK22	WK23	WK24	WK21	WK22	WK23	WK24
Parameter Range Selection																												
Case Setup																												
CFD Simulations																												
Post-Processing																												
Writing and Reporting																												
Post Access Report																												
Post Access Questionnaire																												

Table 2. Test Plan Gantt Chart

6.3 SAFETY

The project will be fully based on numerical modeling and no special safety protocols are necessary.

6.4 CONTINGENCY PLANS

The secondary goal of verifying the use of an open-source code for MHK turbine CFD modeling is an optional goal. The completion of this task will be dependent on the number of shape and spacing iterations required to understand the fairing geometric impacts.

6.5 DATA MANAGEMENT, PROCESSING, AND ANALYSIS

6.5.1 Data Management

The large completed CFD simulation files will temporarily be stored on the NREL HPC, for the duration of the test period. After the test period they will be removed. These files contain the current solution state (velocity, pressure, volume of fluid phase fraction, turbulent kinetic energy, specific turbulent dissipation rate) for every cell in the domain. Each iteration requires on the order of 50 GB of storage, and cannot be kept long term.

Pre-initialization CFD simulation files will be shared with ORPC, along with the corresponding geometry files, for all iterations.

Recorded data will include the loads on the turbine for every time step. The loads will include the force in the x, y, and z direction, and the torque about the rotor axis for all components of the rotor. The recorded loads will be broken by part surfaces including: the support, the shaft, each of the three struts, and 50 span-wise segments for each of the three foils. This recorded data will be stored by NREL and also shared with ORPC as .csv files.

Data submitted to the MHK DR will be normalized with respect to the loads on the base modular geometry. The data submitted to the MHK DR will only include post-processed values for power coefficient and maximum ultimate and fatigue loads on the foils at the strut connections.

6.5.2 Data Processing

Sufficient turbine revolutions will be run to ensure that converged loads are achieved. Previous work found that while the flow patterns on the rotor scale converged quickly, the larger scale effects around

the support structure took longer to develop. For each geometry iteration the solution will be calculated until stable loads are recorded for successive revolutions, and support scale patterns can be identified.

All comparisons between geometric iterations will be relative to the performance of the base modular configuration. This demonstrates the specific impact of the fairing geometry.

6.5.3 Data Analysis

The loads in the simulations will be recorded for small surface segments to learn about the force distributions. The force on the foils will be converted to lift, drag, flap-wise, and edge-wise forces.

Three criteria will be used to evaluate the fairing iterations: net power production, ultimate loads, and fatigue loads. The primary goal of the work is to increase power. Flow acceleration in the original fairing design was small, and interaction effects on the foils decreased lift and subsequently torque. The net power will be tracked for each of the design iterations. A smooth power curve is also beneficial; the influence of the fairing can change what points in the rotation result in the most torque and what the total variability is. The standard deviation of the power will also be tracked and evaluated. Finally, limiting loads on the blades is important for the design. The maximum flap-wise and edge-wise forces on the blades will be tracked. Given the dynamic loading of a cross-flow turbine, fatigue is a large concern, and designs that result in less cyclic loading are favored. The flap-wise and edge-wise loading will be evaluated with a rain flow counter to assess the fatigue properties of the design. These metrics will be evaluated for the full matrix of tested fairing designs.

All simulations will be done at full scale, so no scaling of the data will be performed.

7 PROJECT OUTCOMES

7.1 RESULTS

The work was broken into four main sections: 2D blade-resolved CFD, 2D approaching 3D blade-resolved CFD, 3D blade-resolved CFD, and 3D actuator line CFD. The first three blade-resolved sections were performed using Star-CCM+ and the last actuator line section was performed using OpenFOAM and the turbinesFoam library. Table 3 below gives a brief overview of the four sections, including physical effects captured and computational efficiency.

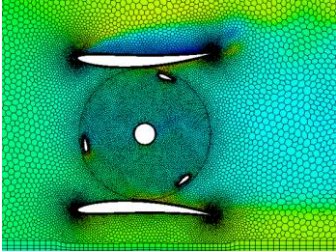
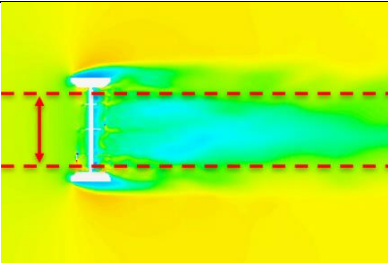
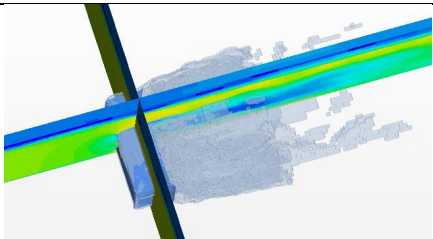
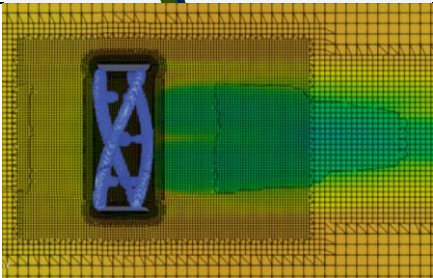
2D Blade-Resolved CFD		<ul style="list-style-type: none"> + High efficiency for large geometric parameter sweep + High fidelity representation of blade flow / dynamic stall - Missing important 3D effects - Different blockage impact
2D → 3D Blade-Resolved CFD		<ul style="list-style-type: none"> • Gradual increase in domain size in spanwise direction to identify sensitive 3D effects + High fidelity representation of blade flow / dynamic stall • Some 3D effects - Different blockage impact
3D Blade-Resolved CFD		<ul style="list-style-type: none"> - Low efficiency for no geometric parameter sweep + High fidelity representation of blade flow / dynamic stall + Captures 3D effects + Captures blockage impact
3D Actuator Line Model CFD		<ul style="list-style-type: none"> + Middle efficiency for some geometric parameter sweep - Low fidelity representation of blade flow / dynamic stall + Captures 3D effects + Captures blockage impact

Table 3. Overview of simulation types used in analysis

2D Blade-Resolved

While there are potentially important 3D physical effects that are not captured, cross-flow turbine architecture can take advantage of reduced mesh sizes with 2D domains. The 2D simulations are the least computationally expensive of the four simulation types used. Rotation to rotation converged loads can be found for a single configuration on average in 1.75 hours of computation time. This relatively small time allowed for a larger sweep of potential support geometries. 323 geometries were tested at the same water depth as the 3D domain, and 280 geometries were tested at a water depth result in an equal blockage as the bare rotor.

The test matrix included two reference fairing geometries; 3D blade-resolved simulations had previously been run for these cross-sectional shapes. Figure 4 shows the results in 5.10 m water depth, matching the water depth and Froude number from the 3D domain. Figure 5 shows the results in 12.96 m water depth, matching the blockage from the 3D domain based on only rotor projected area. In each figure the

horizontal black (Reference 1) and green (Reference 2) lines signify the two reference fairing geometries. All 2D simulations were performed at a single TSR, which was found to have the highest power coefficient in the previously performed 3D blade-resolved CFD simulations.

The geometries are evaluated on the seven criteria given in Table 4. Fatigue equivalent damage values were calculated using Equation 1 where the forces, F , and the cycles, n , are found using a rainflow counter, and the exponent, m , is estimated to be 10 (van Rij, Yu, Edwards, & Mekhiche, 2017)

$$F_{eq} = \sqrt[m]{\sum F_{rainflow}^m n_{rainflow}}$$

Equation 1. Fatigue equivalent damage load Figure 4. 2D blade-resolved CFD in 5.1 m water depth (same depth as 3D domain) normalized metrics as a function of individual support fairing foil parameters. Connected points share all parameters except x-axis parameter.

Mean Power Coefficient
Standard Deviation of Power Coefficient
Maximum Blade Flapwise Force
Maximum Blade Edgewise Force
Blade Flapwise Equivalent Damage
Blade Edgewise Equivalent Damage
Full System Drag

Table 4. Fairing Geometry Normalized Evaluation Criteria

All criteria shown in Figure 4 and Figure 5 are normalized with respect to the largest observed value. Each subplot of the two figures includes all data points, and shows the relationship between one fairing geometry parameter (rows) and one evaluation criteria (columns). The points that are connected have equal fairing geometry parameters for all values except the value on the x-axis, showing the effect of changing only one parameter.

No foil shaped fairing has as high of a mean power coefficient as the reference fairings. The relative performance between the two references is different than expected from previous 3D blade-resolved CFD results. This relative difference highlights the need for a model that can capture the important 3D effects before optimization work.

The trends shown in Figure 4 and Figure 5, based on a domain with the same water depth as the 3D domain and the same blockage as the 3D domain respectively, are not the same. This means that the optimal fairing geometry is a function of the domain. Certain fairing characteristics are more desirable given one blockage and less desirable given a lower blockage. In the matched water depth, with a higher blockage, larger chord lengths and larger thicknesses resulted in an increase in mean power. In the lower matched blockage domain, these two fairing parameters were more weakly correlated to mean power, and had a slightly negative correlation. In most cases an increase in mean power corresponded with an increase in power standard deviation, flapwise maximum and fatigue forces, and edgewise maximum and fatigue forces. There were some blockage specific exceptions. For the lower blockage, while a lower x-position (further upstream) resulted in lower mean power, it resulted in a significantly larger fluctuation in power. Another interesting blockage specific result is the fluctuation in power and maximum edgewise force for the reference fairing geometries. Reference 2, shown in green generates the highest mean power



Testing & Expertise for Marine Energy

for both blockages, but in the lower matched blockage, the standard deviation of power and the maximum edgewise force are lower than Reference 1, and lower than a number of NACA foil fairing geometries, which all produce considerably lower mean power.

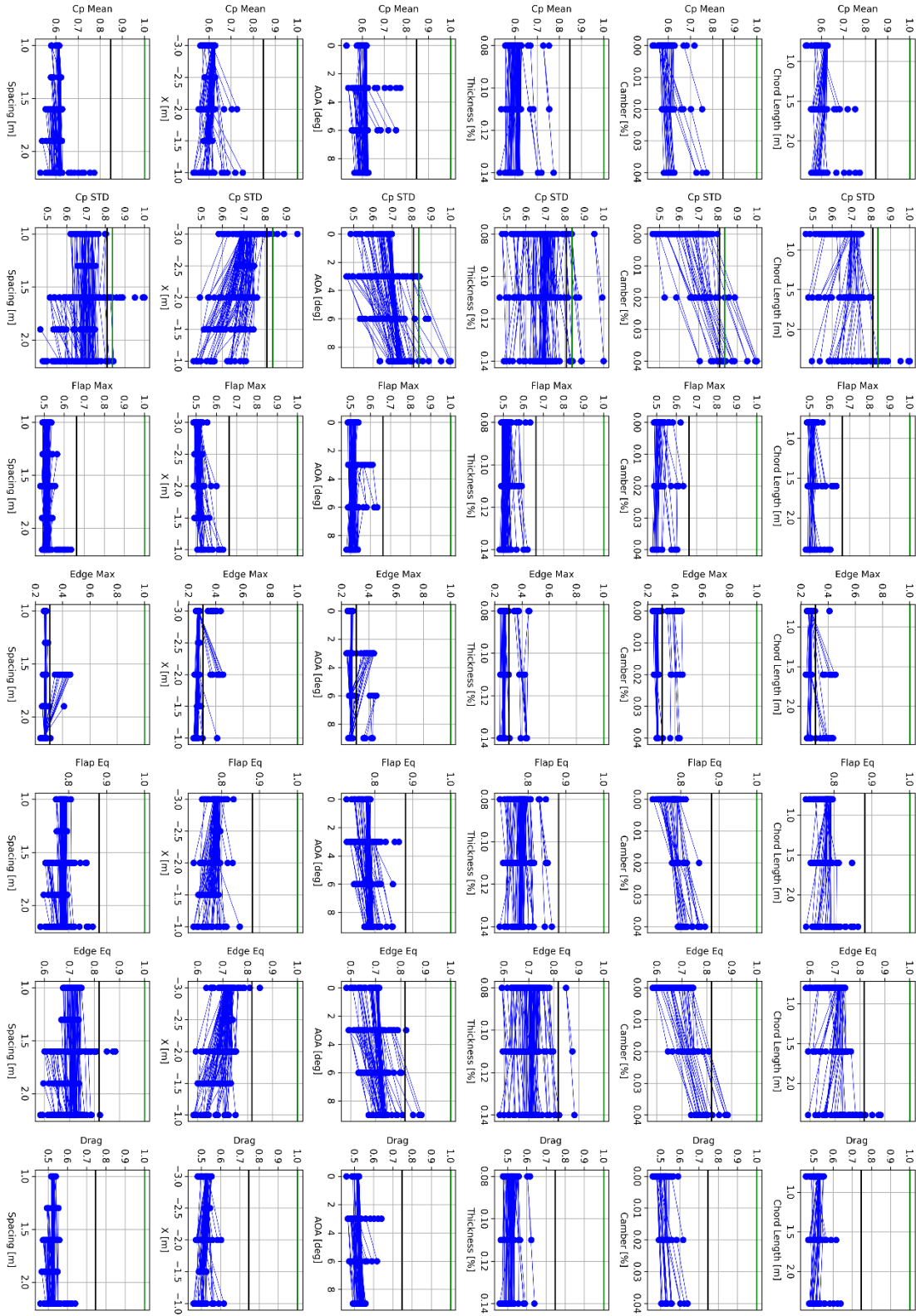


Figure 4. 2D blade-resolved CFD in 5.1 m water depth (same depth as 3D domain) normalized metrics as a function of individual support fairing foil parameters. Connected points share all parameters except x-axis parameter.

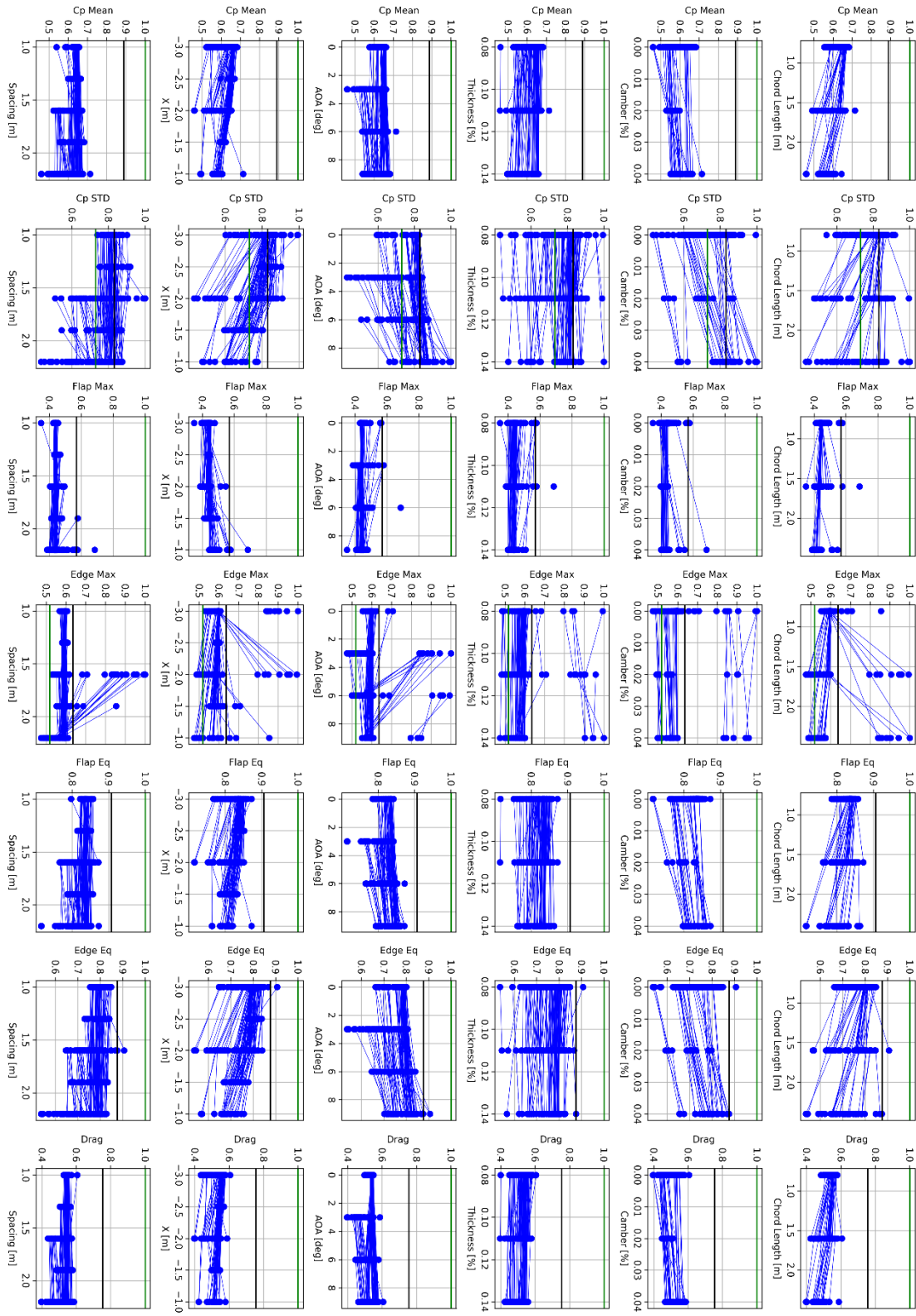


Figure 5. 2D blade-resolved CFD in 12.96 m water depth (same rotor blockage as 3D domain) normalized metrics as a function of individual support fairing foil parameters. Connected points share all parameters except x-axis parameter.

Figure 6 shows the velocity field for the two water depths with the same fairing geometry. The shown foil section is one that results in one of the highest mean powers given the matched depth, shown on the left. While this set of parameters stands out for high mean power when the blockage is higher, it does not when the blockage is matched with a larger water depth.

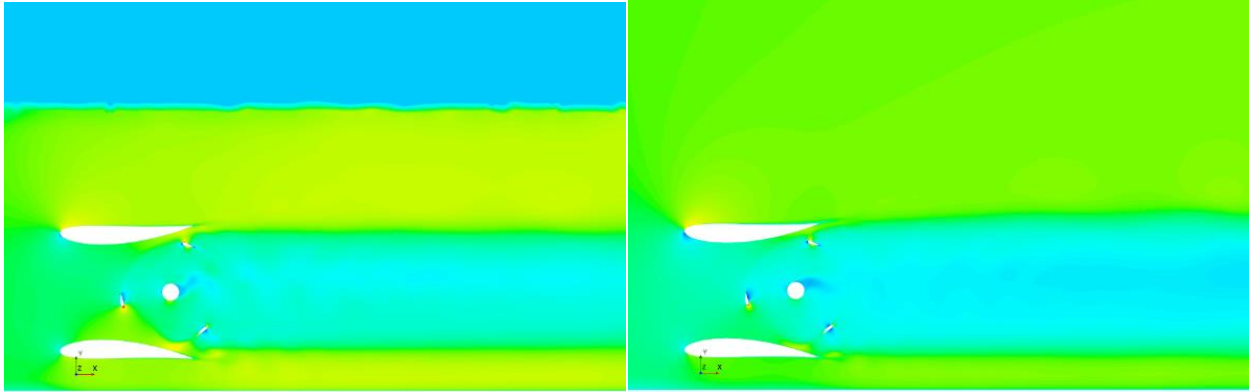


Figure 6. X-direction velocity field with foil fairing shape: $c = 2.4$ m, $m = 4\%$, $p = 50\%$, $t = 14\%$, $aoa = 3$ deg, $x = -2.0$ m, spacing = 2.2m, with matched depth (left) and matched blockage (right)

The differences in trends between Figure 4 and Figure 5 demonstrate the dependence of an optimal fairing design on the domain that it operates in. This can come from a combination of the simple change in blockage as well as more complex flow changes. The relative comparison between Reference 1 and Reference 2 was unexpected based on previously performed 3D blade-resolved CFD results. From the 2D blade-resolved CFD, it is not clear what contribution to the discrepancy comes from different 3D effects.

2D → 3D Blade-Resolved CFD

Simulations were performed with Reference 1 and 2 that progressively stepped from a 2D to a full 3D blade-resolved domain. This included straight extrusions of the 2D mesh in the spanwise direction of one, five, and ten cells. The extruded mesh does not represent the helical shape of the turbine blades, but uses the full 3D set of momentum equations, allowing the transfer and mixing of energy in the spanwise direction. Short sections with a 3D mesh were also tested. This included a length of 0.1 m both with a straight blade section and the true helical blade shape. The full blade span was also tested, including the helical shape of the blades and the struts connecting the blades to the shaft. In this simulation, slip walls were used at the ends of each foil. None of these configurations capture any tip effects, or effects of flow around the fairing in the spanwise direction. All configurations have a constant cross-section for the support structure in spanwise direction; this results in a constant blockage consistent with the 2D domain.

The absolute mean power production for Reference 1 and 2 were both decreased with increasing modeled spanwise length, but the relative performance comparison between the two references was consistent with the 2D domain. This indicates that the difference between the 2D blade-resolved CFD results and the full 3D blade-resolved CFD results is not significantly driven by the 3D effects induced by the helical blades, or the spanwise mixing of momentum. Effects beyond the span of the blades must be important, and the optimal support geometry is a function of these effects. One dominant effect is how the blockage changes with a wider domain. Other effects include the flow around the vertical ends of the support geometry,

and blade tip losses. The ORPC blades have a relatively high aspect ratio, and tip losses are not expected to be dominant. To optimize the support geometry, for a given realistic 3D domain, a 3D simulation is needed.

3D Blade-Resolved CFD

Full 3D blade-resolved CFD simulations are highly computationally expensive for cross-flow turbines. It is not possible to iterate on a large test matrix of geometries. A select set simulations were performed to investigate the influence of some geometry variations of interest. These included tapered extensions of the reference geometries beyond the ends of the rotor, vertical foil shaped sections for the vertical component of the support, no vertical component of the support, and only vertical components of the support with no cross-section along the rotor.

The vertical foil shaped section resulted in a 6% increase in net power compared to the relevant reference geometry. Figure 7 shows the flow field around this iteration. The demonstrated potential for increased power motivated the investigation and optimization of not just the cross section of the support structure, but also the vertical component beyond the rotor.

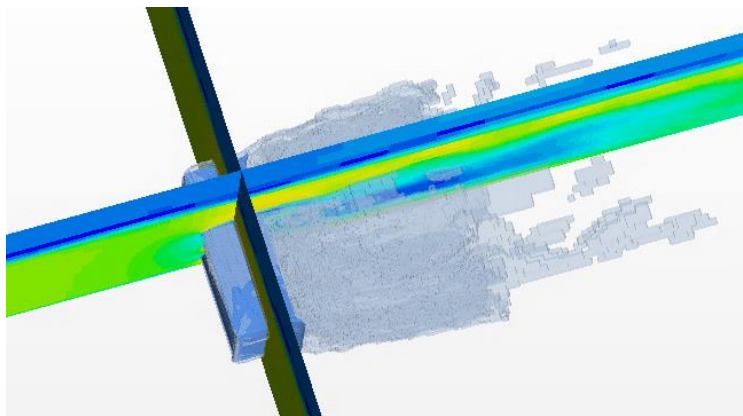


Figure 7. Velocity cross sections and vorticity threshold with support geometry variation with foil shaped vertical components

3D Actuator Line Model CFD

A more expansive investigation of the 3D effects of the full support structure required a more efficient way to model the 3D domain. Actuator line models offer a less computationally expensive option at the cost of decreased accuracy. The decrease in accuracy is particularly difficult for cross-flow turbines, where the results are highly dependent on some form of a dynamic stall model. When an actuator line model is used the flow around the support structure is still fully resolved. The goal is for the actuator line model to capture enough of the blade level physics, and the interaction with the outer support level flow, to be able to optimize the support geometry. Some verification comparisons to blade-resolved simulations are needed. Turbine metrics should be reasonably similar, and the relative trends between different geometries should be well-captured. For these comparisons, Reference 1 and 2 were used as well as a bare rotor.

The selected actuator line model was turbinesFoam, an open-source library for OpenFOAM that is setup to model axial and cross-flow turbines (Bachant, 2023) (Bachant, Goude, & Wosnik, 2018). The inflow

conditions to blade elements are read from the background CFD with a smoothed interpolation centered at the quarter-chord position. The forces and moments on the blade section are calculated and recorded and the corresponding forces and moments on the external flow are added to the background CFD with momentum source terms. The library includes five versions of dynamic stall models as well as an added mass model. It has been previously shown that a version of the Leishman-Beddoes mode for low Mach numbers performs better for the types of flow conditions experienced by cross-flow marine turbines (Sheng, Galbraith, & Coton, 2008) (Dyachuk, Goude, & Bernhoff, 2014). This is the model that Bachant et al. chose for the verification and validation efforts of turbinesFoam. The verification and validation tested the model both with a RANS implementation and a large eddy simulation implementation. The comparisons to experimental data showed a slight overprediction of power at high TSR's, but strong agreement at the peak TSR and below. Thrust was also well-predicted for lower TSR's and slightly overpredicted at high TSR's. The developers of the tool also performed validation of the wake profile (Bachant, Goude, & Wosnik, 2018).

Static polars were generated for the ORPC foil shapes using the panel method tool XFOIL (Drela & Youngren, 2013). The blade was divided into 50 segments along the span, and coefficients were calculated for each section at 8 Reynolds numbers ranging from 50,000 to 5,000,000. The python implementation of the tool AirfoilPrep was used to extend the range of angles of attack for the polars (Ning, 2023). TurbinesFoam uses the generated lift, drag, and moment coefficients. Polars were also defined for the shaft and three different sections of the struts. The geometry of the actuator line follows the helical shape of the blades, and includes the chord length for each of the 50 blade elements. Each of the three struts was broken into 18 elements, with 6 elements extending from the shaft to each of the three blades. The background mesh used the same refinement levels and regions as the previous 3D blade-resolved CFD, which was the result of a dedicated convergence study. The mesh includes some general refinement for the region of the rotor, but none of the blade specific refinements. The total number of cells was reduced from 28 million in the blade-resolved mesh to 2 million in the actuator line mesh. A convergence check was performed for the time step, testing four different time steps (2160, 1080, 540, and 216 dt/revolution). A time step correlating to 1080 time steps per revolution was selected, which was the same time step used in the previous 3D blade-resolved CFD.

Figure 8 shows a representation of the actuator line. The slices in through the three principal planes show the velocity field with a cross-section of the mesh. There is also a threshold surface for momentum source, with a blue to red color indicating the strength of the momentum source. This threshold shows the helical geometry of the actuator line following the ORPC blade.

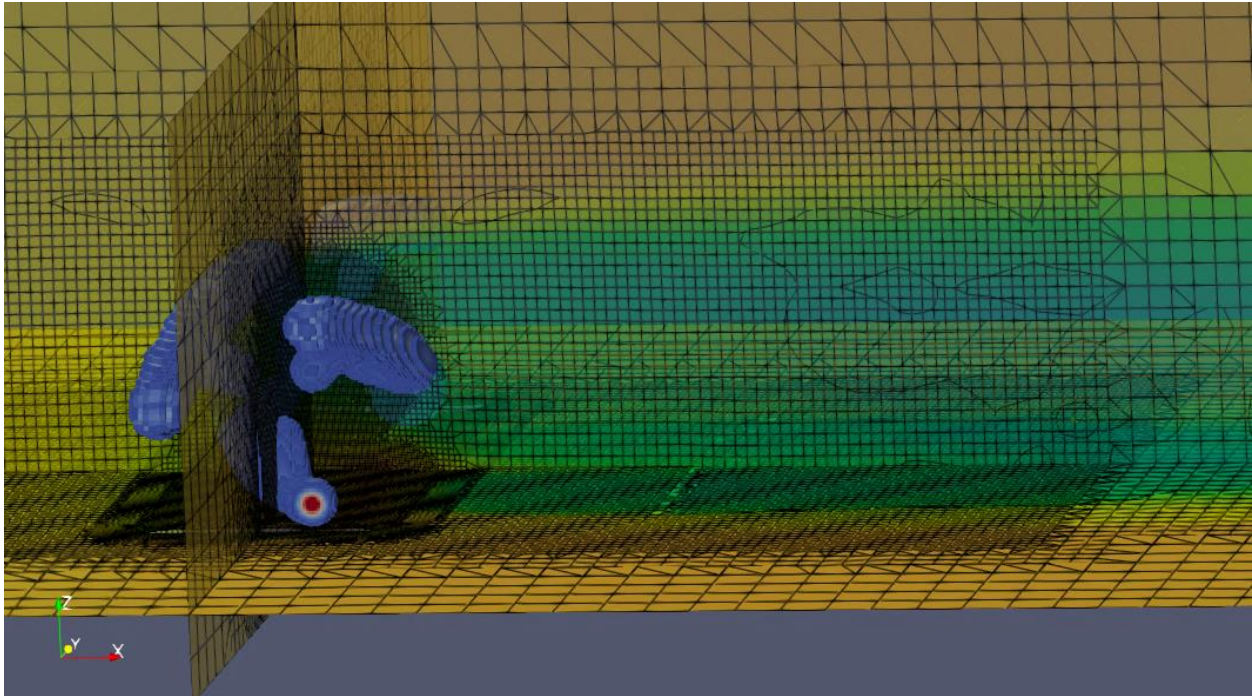


Figure 8. Actuator line (turbinesFoam) source representation and velocity field (OpenFOAM) with reference support structure at a TSR of 3.0

Simulations were run for the two reference supports and the bare rotor for a set of 9 TSR's. The net power and thrust were tracked to ensure that the period-averaged solution had converged to a steady state. This occurred for all conditions after 15 revolutions. The net power, net thrust, and time varying torque were then compared to the solution from the previous 3D blade-resolved CFD for verification. Figure 9 shows the comparison for the period-averaged power and thrust for the actuator line model (ALM) and blade-resolved (BR) results. The comparison does not match the verification and validation results of Bachant et al.; for the ORPC model there is an over prediction of power at low TSR's, and an underprediction of thrust at high TSR's (Bachant, Goude, & Wosnik, 2018). More concerning is the inability to match the TSR with the peak power.

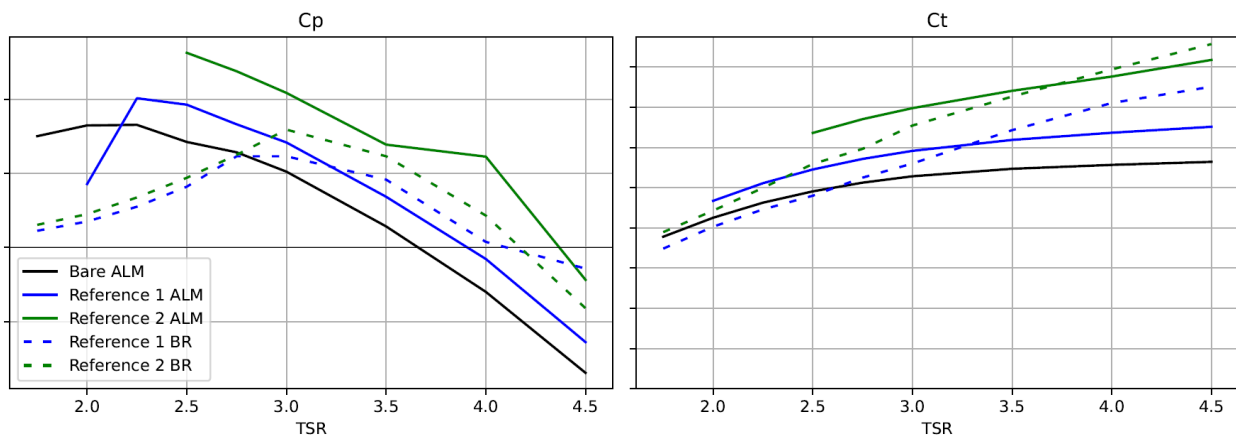


Figure 9. Net power and thrust comparison for actuator line model (ALM) and blade-resolved (BR) CFD simulations with two references and a bare rotor

At lower TSR's the inflow current has a larger component of the relative velocity, resulting in larger changes in angle of attack. Dynamic stall is more likely to be triggered at these lower TSR's where the discrepancy between ALM and BR is greater, both physically and in the numerical model. The disagreement between the ALM and BR results indicate some inaccuracy in the dynamic stall model. Figure 10 shows the same comparison but with the addition of results when the dynamic stall model in turbinesFoam is turned off. There is a general increase in predicted power when the model is not used, higher than expected from the BR curve. However, the predicted peak TSR appears to be a better match. The impact of the dynamic stall model is less significant for the thrust, and the same under prediction of thrust at high TSR's is still present.

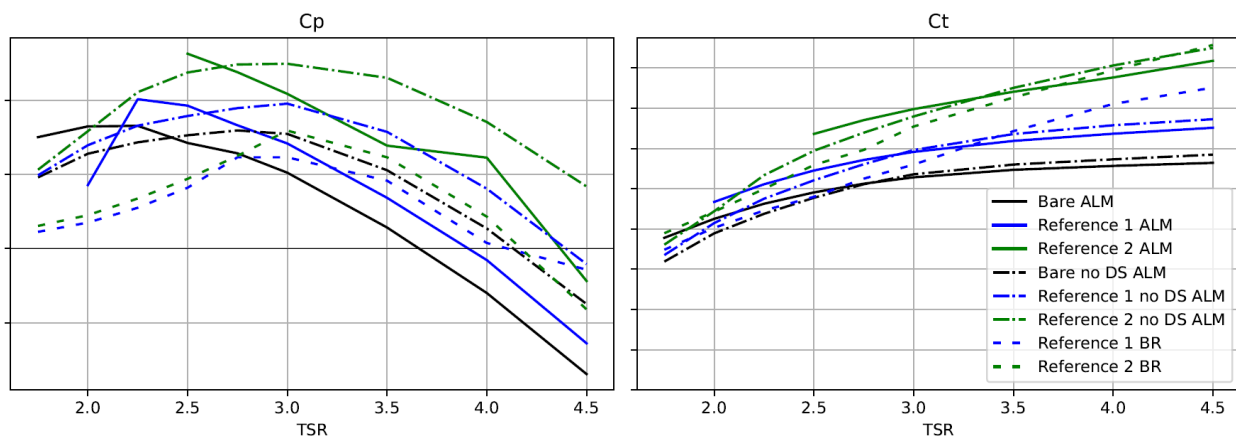


Figure 10. Net power and thrust comparison for actuator line model (ALM) with and without an active dynamic stall model (DS) and blade-resolved (BR) CFD simulations with two references and a bare rotor

The SGC Leishman-Beddoes dynamic stall model implementation in turbinesFoam has 10 standard coefficients that control the four stages of dynamic stall: attached flow, stall, separated flow, and vortex shedding (Sheng, Galbraith, & Coton, 2008) (Bachant P. , 2023). The results shown in Figure 9 use the default values of the coefficients suggested by turbinesFoam, which match the values from the original model development. There is very limited published literature on tuning these parameters to particular applications. Five of the coefficients control the time that each stage of dynamic stall occurs for. It was found that the resulting foil loads are sensitive to these time constants. Dynamic stall allows the lift to temporarily grow larger than the maximum for steady flow conditions. This is followed by a sharp collapse in lift. The time constants were reduced to determine if the stages were lasting longer than physical, resulting in the overpredicted power at low TSR's. The time constant for delayed pressure response, separation point delay, stall onset, and vortex shedding decay were all reduced by the same factor. The time constant for vortex passage was concurrently increased by the same factor. This increase was to prevent repeated vortex shedding, causing subsequent temporary peaks in lift.

Figure 11 shows two iterations of changing the time constants, as well as the default values and the results with no active dynamic stall model. A factor of ten was used for 'T/10', and a factor of two was used for 'T/2'. The torque through a rotation is shown for the bare rotor at three different TSR's. A polar plot is used as a representation of the physical blade rotation. The inflow is from the left (180°) and the rotor

rotation is counterclockwise. The torque is only shown for a single characteristic midspan segment of the blade, so that the load smoothing effects of the helix are not present. At a low TSR of 2.0, where the changes in angle of attack are large, the moment is highly dependent on the model coefficients. The majority of the power is produced on the upstream stroke. In this part of the rotation the effect of changing the time constants is as expected. The three outputs using dynamic stall allow for a higher peak torque and over a longer duration; the shorter time constants result in a quicker collapse in torque. On the downstream stroke the results are unexpected; the longer time constants from the default parameters lead to lower peak torque values and shorter durations. At the near-peak and above-peak TSR's there is little effect of varying the time constants from the default values. The changes in angle of attack are smaller at the higher TSR's, and dynamic stall is less likely to be triggered physically and numerically. At both TSR's there is still a significant change in the torque when the dynamic stall model is fully inactive.

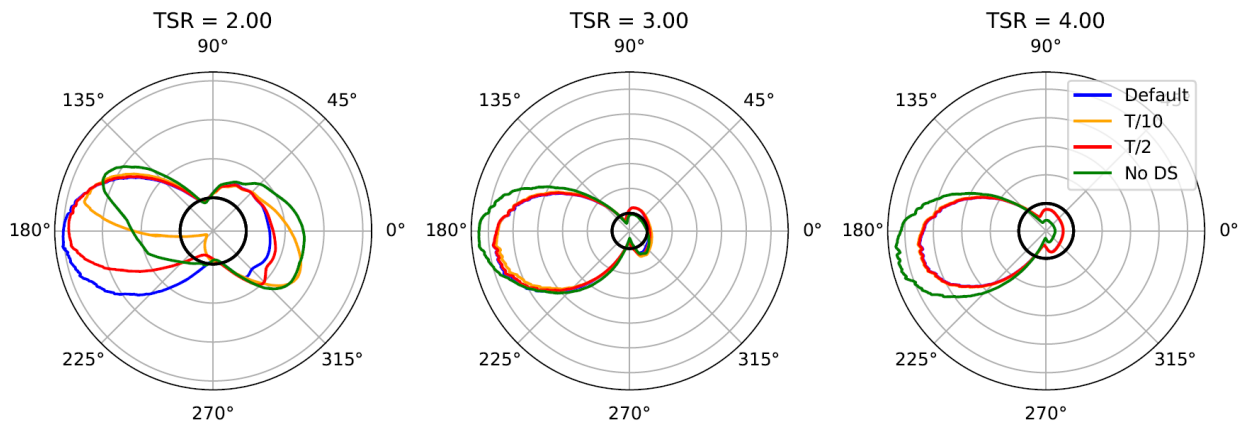


Figure 11. Comparison of varying SGC Leishman-Beddoes dynamic stall parameters on the moment through the rotation at a characteristic midspan section for the bare rotor at different TSR's (upstream = 180°, downstream = 0°, counterclockwise rotation direction)

Figure 12 shows the spanwise distribution of torque for the same load cases presented in Figure 11. The solid line marks the mean torque through the rotation and the dashed lines mark the minimum and maximum. There is some load asymmetry due to the helical blade, but the effects are minimal. The ends of the blades have a large range of moments when the dynamic stall model is active. This only occurs for the below-peak and above-peak TSR's, but not for the near-peak TSR.

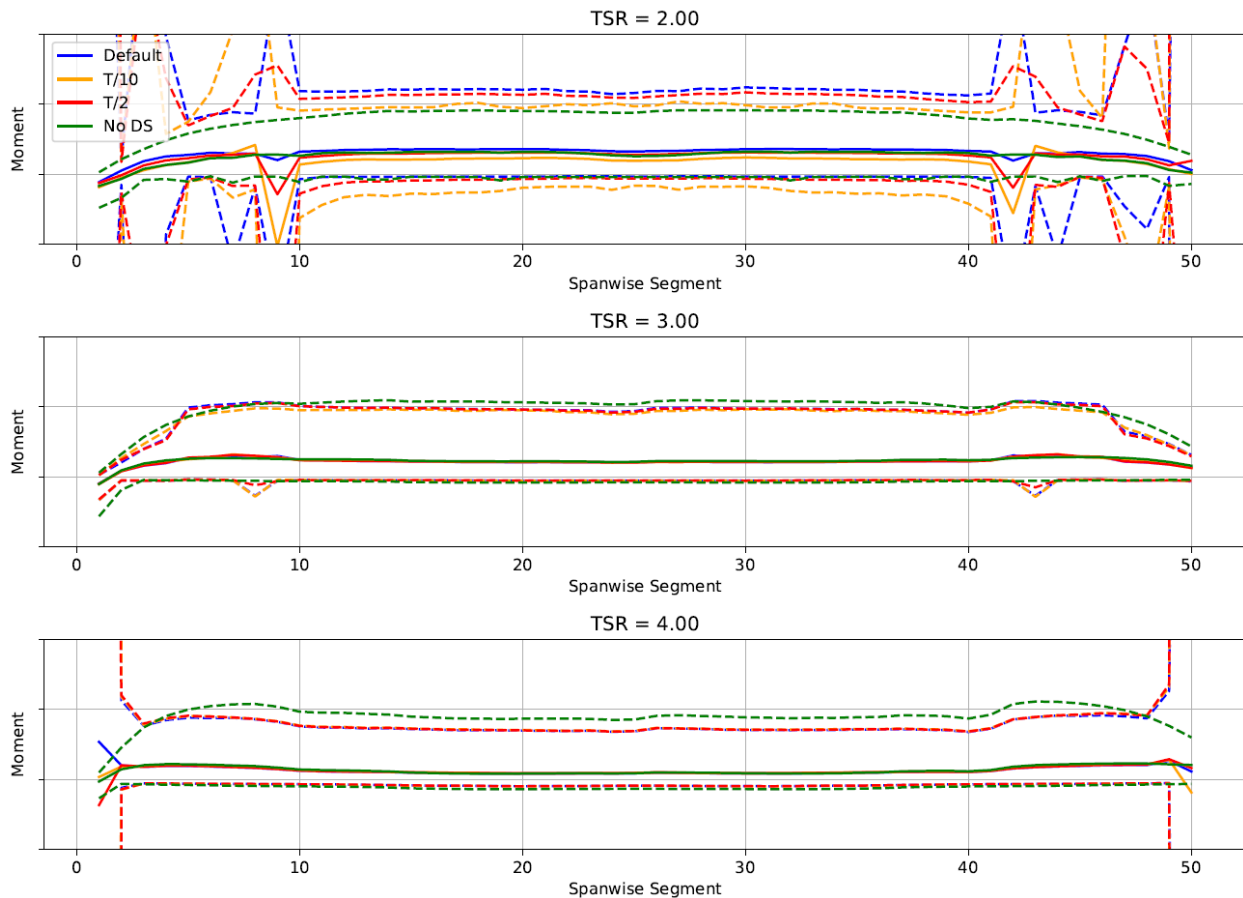


Figure 12. Comparison of varying SGC Leishman-Beddoes dynamic stall parameters on the mean (solid line), minimum, and maximum (dashed lines) moments within a rotation along the span of the blade for the bare rotor at different TSR's

With an expanded project budget, a more thorough investigation of the SGC Leishman-Beddoes coefficients could likely better tune the ALM torque progression to the BR results.

7.2 LESSON LEARNED AND TEST PLAN DEVIATION

There are important differences in performance and flow augmentation depending on the domain. The relative performance of two reference support geometries was found to be inconsistent between 2D and 3D domains. It is expected that blockage contributes significantly to this discrepancy, but other 3D effects are also influential. The same set of foil shaped fairing geometries was tested in a 2D domain with two different water depths, resulting in two different blockage values. The trends in performance were different depending on the depth, indicating that the optimal geometry for one blockage is not the same as the optimal geometry for another blockage. However, even when the blockage of the 2D domain matched the blockage of previously performed 3D CFD, the relative performance of the two references did not match the 3D results. This indicates that there are other critical 3D effects that must be captured to find a true optimal support shape, and a full 3D simulation is needed for the analysis.

3D BR CFD simulations are useful for evaluating the detailed loads of a select set of configurations, but are too computationally expensive for an optimization study. For this reason, a deviation was made to the test plan, and an ALM was setup for the ORPC turbine. The more computationally efficient model can still capture the complex flow patterns around the support and the wake, and some interactions between the outer flow and the rotor flow. The goal was to use this model to optimize the support, and verify the results with 3D blade-resolved CFD. Before running a large set of geometry iterations, a verification study was performed for the solution with two reference geometries, which had previously generated 3D BR results. The power curve match was not as good as desired, so work was put in to tune the dynamic stall model, which was found to be largely impactful on the turbine loads. The implemented dynamic stall model has a large number of parameters, and is difficult to tune well. Improvements should be made to existing dynamic stall models to accurately represent the flow effects that drive cross-flow turbines.

The deviations from the test plan were made to select a better model for support structure optimization. The team did not want to optimize within a framework that didn't represent the realistic physics. The result of an optimization is a function of the model type. These changes and additions to the plan used a significant portion of the budget, limiting the total simulations that could be run.

8 CONCLUSIONS AND RECOMMENDATIONS

Flow augmentation in confined channels is highly dependent on the domain. Not only is the performance dependent on the domain, but the fairing geometry resulting in the optimal performance is different depending on the extents of the channel. This was first demonstrated in the 2D CFD analysis. The performance, quantified by mean power, variation in power, maximum blade loads, and fatigue blade loads, follow function of a set of fairing parameters. The trends between the performance and parameters are inconsistent when modeled at two different water depths. The geometry that would be selected as optimal at one depth is not the same that would be selected at a different depth. It is expected that a large part of this domain dependency can be treated as a function of blockage.

Beyond the impacts of blockage, differences in the load comparisons with two different geometries were found between a 2D and 3D domain. Optimization of flow augmentation structures for turbines should be done in a representative domain. This was shown specifically for a cross-flow turbine, but it is expected that the same is true for axial flow devices.

Cross-flow turbines are more computationally expensive to model, and many geometric iterations are not feasible with a blade-resolved 3D domain. Actuator line models within CFD offer potential for outer flow acceleration optimization, however the predicted performance is highly dependent on dynamic stall models. The current state-of-the-art dynamic stall model with default parameters does not accurately predict the hydrodynamic loads for the analyzed turbine. Work should be done to improve methods of tuning the SGC Leishman-Beddoes model, or improvements should be made to the model itself.

In the 2D domain, there were no improvements to the net power compared to the references. A 6% improvement in net power was achieved with a variation to the vertical end of the support. A verified actuator line model was needed for a more expansive investigation of this potential.

Some logical next steps would be to try to improve the accuracy of the dynamic stall model implemented in the actuator line code. This could involve the use of a multi-disciplinary optimization to efficiently tune the model parameters to best match blade-resolved CFD load histories. The implementation of a custom dynamic stall model developed for the specific turbine could also be explored. A multi-disciplinary optimization could then efficiently explore 3D fairing geometry parameters using the actuator line model to help improve the performance of the support structure in a realistic 3D domain.

9 REFERENCES

- Bachant, P. (2023). *turbinesFoam*. Retrieved from github:
<https://github.com/turbinesFoam/turbinesFoam>
- Bachant, P., Goude, A., & Wosnik, M. (2018). Actuator line modeling of vertical-axis turbines.
doi:<https://doi.org/10.48550/arXiv.1605.01449>
- Drela, M., & Youngren, H. (2013). *XFOIL Subsonic Airfoil Development System*.
- Dyachuk, E., Goude, A., & Bernhoff, H. (2014). Dynamic Stall Modeling for the Conditions of Vertical Axis Wind Turbines. *American Institute of Aeronautics and Astronautics Journal*.
doi:<https://doi.org/10.2514/1.J052633>
- Garanovic, A. (2022, 5 20). *ORPC Picks Turbine Shafts Supplier for Tidal Power Systems*. Retrieved from Offshore Energy Biz: <https://www.offshore-energy.biz/orpc-picks-turbine-shafts-supplier-for-tidal-power-systems/>
- ORPC. (2023, 2 1). *RIVGEN® Power System & Integrated Microgrid Solutions*. Retrieved from <https://orpc.co/rivgen-power-system-integrated-microgrid-solutions/>
- Sheng, W., Galbraith, R., & Coton, F. (2008). A Modified Dynamic Stall Model for Low Mach Numbers. *Journal of Solar Energy Engineering*.
- van Rij, J., Yu, Y.-H., Edwards, K., & Mekhiche, M. (2017). Ocean power technology design optimiation. *International Journal of Marine Energy*, 20, 97-108.
doi:<https://doi.org/10.1016/j.ijome.2017.07.010>

10 ACKNOWLEDGEMENTS

A portion of the research was performed using computational resources sponsored by the Department of Energy's Office of Energy Efficiency and Renewable Energy and located at the National Renewable Energy Laboratory.

This work was authored by the National Renewable Energy Laboratory, operated by Alliance for Sustainable Energy, LLC, for the U.S. Department of Energy (DOE) under Contract No. DE-AC36-08GO28308. Funding provided by the DOE Water Power Technologies Office. The views expressed in the



Testing & Expertise for Marine Energy

article do not necessarily represent the views of the DOE or the U.S. Government. The U.S. Government retains and the publisher, by accepting the article for publication, acknowledges that the U.S. Government retains a nonexclusive, paid-up, irrevocable, worldwide license to publish or reproduce the published form of this work, or allow others to do so, for U.S. Government purposes.